Second-order nonlinear optical properties of Λ-shaped pyrazine derivatives

Castet, Frédéric; Gillet, Adrien; Bureš, Filip; Plaquet, Aurélie; Rodriguez, Vincent; Champagne, Benoît

Published in:
Dyes and pigments

DOI:
10.1016/j.dyepig.2020.108850

Publication date:
2021

Document Version
Publisher's PDF, also known as Version of record

Dyes and Pigments 184 (2021) 108850

Contents lists available at ScienceDirect

Dyes and Pigments

journal homepage: http://www.elsevier.com/locate/dyepig

Second-order nonlinear optical properties of Λ-shaped pyrazine derivatives

Frédéric Castet [a,*], Adrien Gillet [a], Filip Bureš [b], Aurélie Plaquet [c], Vincent Rodriguez [a,**], Benoît Champagne [c,***]

[a] Institut des Sciences Moléculaires (ISM, UMR CNRS 5255), Université de Bordeaux, 351 Cours de La Libération, 33405, Talence, France
[b] Institute of Organic Chemistry and Technology, Faculty of Chemical Technology, University of Pardubice, Studentská 573, Pardubice, 532 10, Czech Republic
[c] Unité de Chimie Physique Théorique et Structurale, Chemistry Department, Namur Institute of Structured Matter, University of Namur, Rue de Bruxelles, 61, B-5000, Namur, Belgium

ARTICLE INFO

Keywords:
Pyrazines
Nonlinear optics
Hyper-Rayleigh scattering
First hyperpolarizability
Kleinman symmetry
Density functional theory

ABSTRACT

The linear and nonlinear optical (NLO) properties of a series of Λ-shaped derivatives containing a 4,5-dicyanopyrazine acceptor unit, *N,N*-dimethylamino donor groups and systematically enlarged π-conjugated linkers are investigated by means of UV/Visible and Hyper-Rayleigh scattering spectroscopies. Density functional theory calculations are also carried out to rationalize the magnitude and symmetry of the NLO responses. The results demonstrate that these compounds possess two low-lying excited electronic states close to each other in energy, which are accessible through one-photon optical transitions respectively polarized perpendicular and parallel to the two-fold molecular axis. These two states contribute additively to the first hyperpolarizability, which exhibits a dominant dipolar character. We also show that the NLO responses significantly deviate from Kleinman's index permutation symmetry.

1. Introduction

The design of organic chromophores having the ability to deliver large second order nonlinear optical (NLO) responses has been a continuous source of research for the past thirty years, in connection with a broad field of applications ranging from smart materials (including optical telecommunications, data storage, information and signal processing) [1,2] to biology (including *in vivo* bioimaging and therapy) [3–6]. Most of systems reported to date are (one-dimensional) dipolar compounds, which comprise a π-conjugated linker connected at both ends to electron-donating (D) and electron-withdrawing (A) chemical substituents. Varying the nature of the D/A groups and the length of the π-conjugated bridge by means of chemical design remains the most common strategy for tuning the magnitude of the first hyperpolarizability (β) [7–15].

However, if 1D compounds present the advantage to enable electric-field poling in chromophore-polymer composite materials [1], they are limited by the fact that any increase of the first hyperpolarizability is most often accompanied by a redshift of the absorbance maxima, which translates into a loss of transparency. An alternative to circumvent the nonlinearity/transparency tradeoff is to exploit the dimensionality of the NLO chromophores. In that respect, two-dimensional octupolar chromophores that exhibit three-fold symmetry, with crystal violet as prototypical compound, have proven to be of major interest for electro-optics, since their potentially high β values are associated with a zero dipole moment and with increased transparency [16–18]. The enhanced nonlinear response of these compounds originates from the existence of two degenerate low-lying excited states accessible by one-photon absorption, which both contribute to the first hyperpolarizability.

NLO chromophores exhibiting C_{2v} symmetry with a rigid Λ-shaped geometry also enable the possibility of modulating the magnitudes and dimensionality of the second order NLO responses, and offer an interesting compromise combining the advantages of 1D and 2D systems [19–23]. As exemplified by 3,5-dinitro-aniline [24] or (dicyanomethylene)pyran derivatives [25], NLO compounds with C_{2v} symmetry possess two low-lying excited electronic states close to each other in energy, the first transition (S_1) being polarized perpendicular to the symmetry (z) axis (*i.e.* along x), whereas the second (S_2) is polarized parallel to z. As a consequence, the β tensor contains two main

* Corresponding author.
** Corresponding author.
*** Corresponding author.
E-mail address: frederic.castet@u-bordeaux.fr (F. Castet).

https://doi.org/10.1016/j.dyepig.2020.108850
Received 4 August 2020; Received in revised form 9 September 2020; Accepted 10 September 2020
Available online 16 September 2020

components, β_{zzz}, which in a Sum-Over-States (SOS) picture depends only on S_2, and β_{zxx}, which depends both on S_1 and S_2. Important aspects related to the large β_{zxx} components lie in the fact that harmonic lights polarized perpendicular to the transition dipole are not reabsorbed, which reduces losses in the second-harmonic intensity, and that fundamental and harmonic lights are propagating with different polarization, which offers the possibility of phase-matching. Theoretical investigations further demonstrated that specific ratios between the off-diagonal (β_{zxx}) and diagonal (β_{zzz}) tensor components can be achieved by finely tuning the D/A strengths and the angle between the two molecular branches [26,27]. In addition, it has been evidenced that the presence of the low-lying excited state with transition dipole perpendicular to the symmetry axis was responsible for significant deviation from Kleinman's index permutation symmetry [24,28].

Herein, we report a detailed investigation of the linear and nonlinear optical properties of a series of Λ-shaped pyrazine derivatives [29], which involve systematically enlarged π-conjugated segments with 1, 4-phenylene rings as well as acetylene units (Fig. 1). Our study combines Hyper-Rayleigh Scattering (HRS) measurements to Density Functional Theory (DFT) calculations, and focuses on the impact of the nature and length of the π-conjugated system on the magnitude and symmetry of the second-order NLO response, in relation with the structural symmetry of the compounds. In particular, we introduce a new experimental approach to evaluate the deviations from Kleinman's symmetry, which are interpreted in the light of theoretical calculations.

2. Experimental and theoretical details

2.1. Hyper-Rayleigh Scattering measurements

UV/vis absorption spectra were recorded on a PerkinElmer Lambda 650 spectrophotometer in dichloromethane (DCM). HRS experiments were performed on diluted solutions with concentrations ranging from 10^{-4} to 10^{-5} mol/L in DCM, checking the linear dependence of absorbance. The first hyperpolarizability was determined from the intensity of the incoherent scattered light at the second harmonic frequency of an IR diode pumped picosecond laser Nd:YVO_4 ($\lambda = 1064$ nm, pulse duration 65 ps, repetition rate 2 kHz). The scattered light was collected at 90° and focused into a Jobin–Yvon Horiba spectrograph, according to an experimental setup reported previously [30].

The HRS signal of incoherent and uncorrelated molecular scatterers in dilute solution is related to the molecular first hyperpolarizability as follows:

$$I^{2\omega} \propto C_{chr}\langle\beta^2_{HRS}\rangle(I^{\omega})^2 \times 10^{-\varepsilon_{2\omega}\ell C_{chr}} \quad (1)$$

where I^{ω} is the intensity of the incident light beam of frequency ω and C_{chr} is the concentration of the NLO chromophores. The last term (where $\varepsilon_{2\omega}$ is the molar extinction coefficient at frequency 2ω and ℓ the optical path length) accounts for the absorption losses at the second harmonic wavelength. $\langle\beta^2_{HRS}\rangle$ is the orientational average of the first hyperpolarizability tensor over all possible molecular orientations. Since for a non-polarized/natural incident light both horizontal (H ∥ X) and vertical (V ∥ Z) polarizations have equal weights, β_{HRS} can be expressed as the

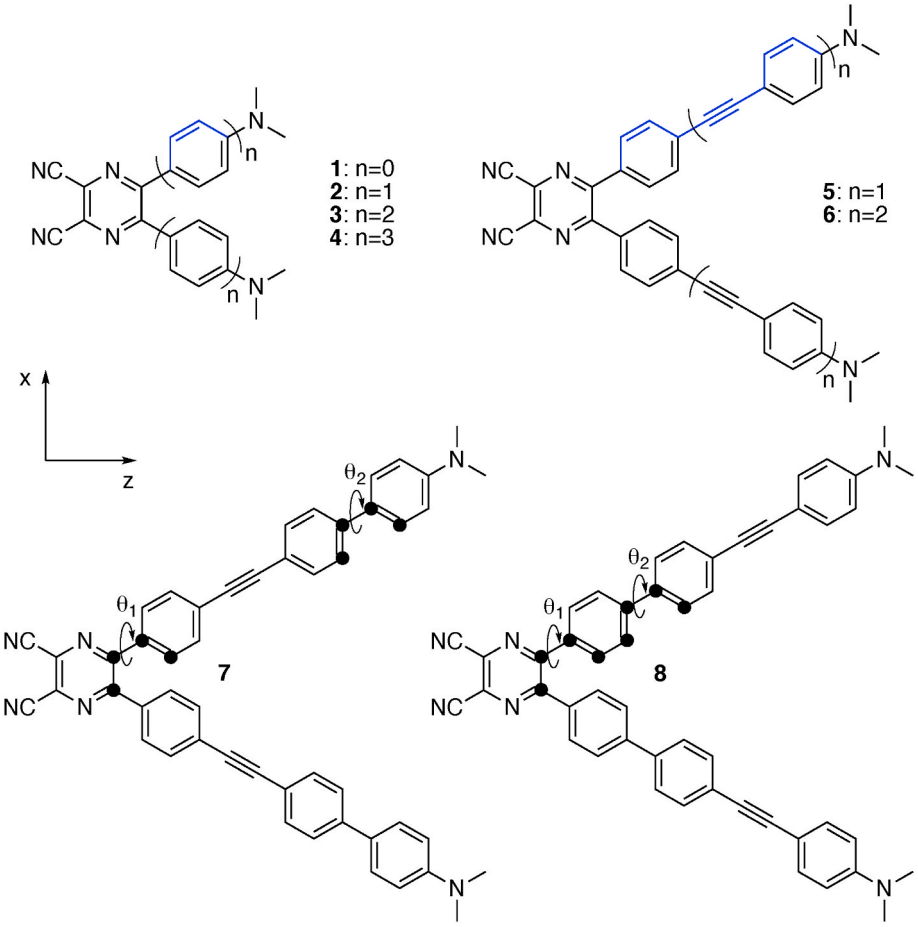

Fig. 1. Pyrazine derivatives investigated in this work. The Cartesian frame used in NLO calculations is shown on the left. The dihedral angles around single bonds (θ_{1-3}) are defined between dotted carbon atoms starting from the pyrazine core, as exemplified on compounds **7** and **8**. The conjugated segment considered to compute the BLA is shown in blue in compounds **1**–**6**.

sum of two contributions:

$$\beta_{HRS} = \beta_{HRS}(-2\omega;\omega,\omega) = \sqrt{\langle\beta^2_{HRS}\rangle} = \sqrt{\langle\beta^2_{ZZZ}\rangle + \langle\beta^2_{ZXX}\rangle} \tag{2}$$

The $\langle\beta^2_{ZZZ}\rangle$and $\langle\beta^2_{ZXX}\rangle$ invariants can be written in terms of molecular β tensor components as follows:

$$\begin{aligned}\langle\beta^2_{ZZZ}\rangle = &\tfrac{1}{7}\sum_{\zeta}^{x,y,z}\beta^2_{\zeta\zeta\zeta} + \tfrac{4}{35}\sum_{\zeta\neq\eta}^{x,y,z}\beta^2_{\zeta\zeta\eta} + \tfrac{2}{35}\sum_{\zeta\neq\eta}^{x,y,z}\beta_{\zeta\zeta\zeta}\beta_{\zeta\eta\eta} \\ &+\tfrac{4}{35}\sum_{\zeta\neq\eta}^{x,y,z}\beta_{\eta\zeta\zeta}\beta_{\zeta\zeta\eta} + \tfrac{4}{35}\sum_{\zeta\neq\eta}^{x,y,z}\beta_{\zeta\zeta\zeta}\beta_{\eta\eta\zeta} + \tfrac{1}{35}\sum_{\zeta\neq\eta}^{x,y,z}\beta^2_{\eta\zeta\zeta} \\ &+\tfrac{4}{105}\sum_{\zeta\neq\eta\neq\xi}^{x,y,z}\beta_{\zeta\zeta\eta}\beta_{\eta\xi\xi} + \tfrac{1}{105}\sum_{\zeta\neq\eta\neq\xi}^{x,y,z}\beta_{\eta\zeta\zeta}\beta_{\eta\xi\xi} \\ &+\tfrac{4}{105}\sum_{\zeta\neq\eta\neq\xi}^{x,y,z}\beta_{\zeta\zeta\eta}\beta_{\xi\xi\eta} \\ &+\tfrac{2}{105}\sum_{\zeta\neq\eta\neq\xi}^{x,y,z}\beta^2_{\zeta\eta\xi} + \tfrac{4}{105}\sum_{\zeta\neq\eta\neq\xi}^{x,y,z}\beta_{\zeta\eta\xi}\beta_{\eta\zeta\xi}\end{aligned} \tag{3}$$

$$\begin{aligned}\langle\beta^2_{ZXX}\rangle = &\tfrac{1}{35}\sum_{\zeta}^{x,y,z}\beta^2_{\zeta\zeta\zeta} + \tfrac{4}{105}\sum_{\zeta\neq\eta}^{x,y,z}\beta_{\zeta\zeta\zeta}\beta_{\zeta\eta\eta} - \tfrac{2}{35}\sum_{\zeta\neq\eta}^{x,y,z}\beta_{\zeta\zeta\zeta}\beta_{\eta\eta\zeta} \\ &+\tfrac{8}{105}\sum_{\zeta\neq\eta}^{x,y,z}\beta^2_{\zeta\zeta\eta} + \tfrac{3}{35}\sum_{\zeta\neq\eta}^{x,y,z}\beta^2_{\zeta\eta\eta} - \tfrac{2}{35}\sum_{\zeta\neq\eta}^{x,y,z}\beta_{\zeta\zeta\eta}\beta_{\eta\zeta\zeta} \\ &+\tfrac{1}{35}\sum_{\zeta\neq\eta\neq\xi}^{x,y,z}\beta_{\zeta\eta\eta}\beta_{\zeta\xi\xi} - \tfrac{2}{105}\sum_{\zeta\neq\eta\neq\xi}^{x,y,z}\beta_{\zeta\zeta\xi}\beta_{\eta\eta\xi} \\ &-\tfrac{2}{105}\sum_{\zeta\neq\eta\neq\xi}^{x,y,z}\beta_{\zeta\zeta\eta}\beta_{\eta\xi\xi} \\ &+\tfrac{2}{35}\sum_{\zeta\neq\eta\neq\xi}^{x,y,z}\beta^2_{\zeta\eta\xi} - \tfrac{2}{105}\sum_{\zeta\neq\eta\neq\xi}^{x,y,z}\beta_{\zeta\eta\xi}\beta_{\eta\zeta\xi}\end{aligned} \tag{4}$$

Experimentally, $\langle\beta^2_{ZZZ}\rangle$ and $\langle\beta^2_{ZXX}\rangle$ can be obtained independently from measurements performed in the VV (vertically polarized incident and scattered lights) and HV (horizontally polarized incident light and vertically polarized scattered light) configurations, respectively. Their ratio, referred to as the depolarization ratio (DR), depends on the symmetry of the NLO chromophores and ranges between 1.5 for octupolar compounds and 9 for pure dipolar molecules [31]:

$$DR = \frac{\langle\beta^2_{ZZZ}\rangle}{\langle\beta^2_{ZXX}\rangle} \tag{5}$$

However, more accurate determination of β_{HRS} and DR are obtained by considering the full range of polarization angles Ψ of the incident light. Considering a phase retardation of $\pi/2$ in accordance with the experimental setup (which combines a rotating half-wave plate and a fixed quarter-wave plate, see Ref. 30 for details), the intensity of the harmonic light collected perpendicular to the incident beam and vertically polarized implies a quartic dependence in cosΨ, following the expression established by Bersohn [32]:

$$\begin{aligned}I^{2\omega}_{\Psi V} \propto &\langle\beta^2_{ZXX}\rangle\cos^4\Psi + \langle\beta^2_{ZZZ}\rangle\sin^4\Psi \\ &+\langle(\beta_{ZXZ}+\beta_{ZZX})^2 - 2\beta_{ZZZ}\beta_{ZXX}\rangle\cos^2\Psi\sin^2\Psi\end{aligned} \tag{6}$$

In number of previously reported works [12,24,25,28,30], NLO measurements of rod-like and Λ-shaped compounds were analyzed assuming a planar C_{2v} molecular symmetry (where the molecules lay in a mean xz plane with z the twofold symmetry axis), as well as time reversibility of the second-order optical process. The latter approximation, known as Kleinman's symmetry, is strictly fulfilled only in the static limit and assumes the invariance of the β tensor components with respect to permutation of their Cartesian indices, such that $\beta_{ijk} = \beta_{kji}$. Assuming both planar C_{2v} and Kleinman symmetries implies that $\beta_{zyy} = \beta_{yyz} = 0$, $\beta_{zzz} \neq 0$ and $\beta_{zxx} = \beta_{xxz} \neq 0$ in equations (3) and (4). The intensity of the harmonic light given in equation (6) can then be expressed as a function of the two non-zero independent β components:

$$\begin{aligned}I^{2\omega}_{\Psi V}(C_{2v}) \propto &\frac{1}{105}\beta^2_{zzz}\left(\left(15+18R+27R^2\right) - \left(24+68R+4R^2\right)\cos^2\Psi\right. \\ &\left.+\left(12+48R-12R^2\right)\cos^4\Psi\right)\end{aligned} \tag{7}$$

where $R = \beta_{zxx}/\beta_{zzz}$. Accordingly, the expressions of β_{HRS} and DR can be simplified into:

$$\beta_{HRS}(C_{2v}) = |\beta_{zzz}|\left(\frac{6}{35}+\frac{16}{105}R+\frac{38}{105}R^2\right)^{1/2} \tag{8}$$

$$DR(C_{2v}) = \frac{\frac{1}{7}+\frac{6}{35}R+\frac{9}{35}R^2}{\frac{1}{35}-\frac{2}{105}R+\frac{11}{105}R^2} \tag{9}$$

In the work reported herein, we rely on spherical harmonics in addition to Cartesian coordinates. This formalism, in which the first hyperpolarizability is decomposed in terms of dipolar ($\beta_{J=1}$) and octupolar ($\beta_{J=3}$) tensorial components, allows us to analyze the HRS data without imposing any structural symmetry constraint on the β tensor. Assuming Kleinman's conditions, the three HRS invariants of equation (6), $\langle\beta^2_{ZZZ}\rangle$, $\langle\beta^2_{ZXX}\rangle$ and $\langle(\beta_{ZXZ}+\beta_{ZZX})^2 - 2\beta_{ZZZ}\beta_{ZXX}\rangle$, can be rewritten as:

$$\langle\beta^2_{ZZZ}\rangle = |\beta_{J=1}|^2\left(\frac{9}{45}+\frac{6}{105}\rho^2\right) \tag{10}$$

$$\langle\beta^2_{ZXX}\rangle = |\beta_{J=1}|^2\left(\frac{1}{45}+\frac{4}{105}\rho^2\right) \tag{11}$$

$$\langle(\beta_{ZXZ}+\beta_{ZZX})^2 - 2\beta_{ZZZ}\beta_{ZXX}\rangle = |\beta_{J=1}|^2\left(-\frac{2}{45}+\frac{22}{105}\rho^2\right) \tag{12}$$

where the nonlinear anisotropy parameter $\rho = |\beta_{J=3}|/|\beta_{J=1}|$ denotes the relative magnitude of the octupolar and dipolar contributions to the first hyperpolarizability. The total HRS intensity and the depolarization ratio are expressed as:

$$\beta_{HRS} = |\beta_{J=1}|\sqrt{\frac{2}{3}\left(\frac{1}{3}+\frac{1}{7}\rho^2\right)} \tag{13}$$

$$\mathrm{DR} = \frac{9\left(1+\frac{2}{7}\rho^2\right)}{1+\frac{12}{7}\rho^2} \tag{14}$$

and equation (6) becomes:

$$I^{2\omega}_{\Psi V} \propto |\beta_{J=1}|^2\left(\frac{1}{45}+\frac{4}{105}\rho^2\right)\left[\cos^4\Psi + \Delta\sin^4\Psi + \Delta'\cos^2\Psi\sin^2\Psi\right] \tag{15}$$

According to Kleinman symmetry, $\Delta = DR$ and $\Delta' = 7 - DR$. Since the ρ and DR parameters are linked through equation (14), the values of the two parameters can be determined from the polarization curves by using a fitting procedure implying ρ as the only adjustable parameter. Assuming in addition that molecular structures have a C_{2v} symmetry, the ρ and DR parameters evolve as a function of $R = \beta_{zxx}/\beta_{zzz}$ as shown in Fig. 2.

Finally, to address the applicability of the time-reversibility assumption, it is further possible to evaluate the deviation from the Kleinman symmetry by introducing an additional parameter in equation (15), in such a way that $\Delta = DR_{NK}$ and $\Delta' = 7 - DR_{NK} + \delta_{NK}$. In this case, the "non-Kleinman" (NK) depolarization ratio, DR_{NK}, and the deviation from Kleinman symmetry, δ_{NK}, are optimized according to a two-parameter fitting procedure.

2.2. Quantum chemical calculations

Molecular structures were optimized at the density functional theory (DFT) level using the hybrid *meta*-GGA M06–2X exchange-correlation functional (XCF) including 54% of Hartree-Fock (HF) exchange, in association with the 6-311G(d) basis set. Real values for all vibrational

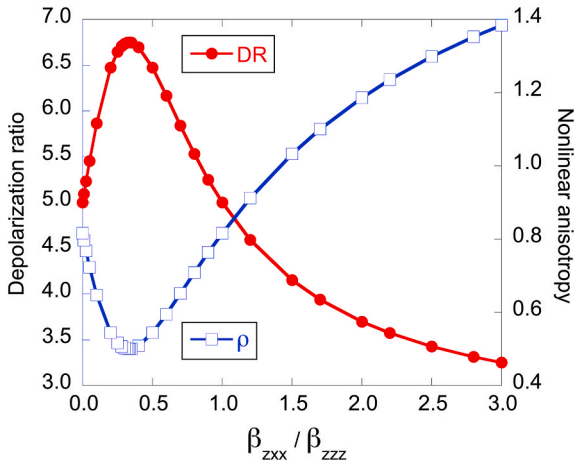

Fig. 2. Evolution of the depolarization and anisotropy ratios as a function of $R = \beta_{zxx}/\beta_{zzz}$ when assuming both C_{2v} and Kleinman symmetries (equations (9) and (14)).

frequencies confirmed that the geometries correspond to minima on the potential energy surface. Linear and nonlinear optical properties (in the static limit and using an incident wavelength of 1064 nm) were determined using time-dependent (TD) DFT with the same functional and the larger 6-311+G(d) basis set containing additional diffuse functions. The M06–2X XCF was demonstrated to perform well for calculating the second-order NLO properties of a large variety of organic chromophores [33–37]. Solvent effects were taken into account in both geometry optimizations and calculations of the optical responses by using the integral equation formalism of the polarizable continuum model (IEF-PCM) [38], with dichloromethane as solvent. All calculations were performed using the Gaussian09 program package [39].

3. Results and discussion

3.1. Structural and ground-state electronic properties

All molecules exhibit a C_2 symmetry. The bond length alternation (BLA) along the conjugated chain connecting the donor and acceptor units (*i.e.* between the most distant carbon atoms of the first and last phenyl units, see Fig. 1), as well as the torsional angles around single bonds (between the pyrazine and phenyl rings and between consecutive phenyl units when relevant), are listed in Table 1 for all compounds. The energy of the frontier MOs and the ground-state dipole moments are also provided, together with the net charge δ of the *N,N*-dimethylamino donor and dicyano-pyrazine acceptor moieties (calculated by summing the Mulliken atomic populations). For a conjugated chain containing *N* carbon atoms, the BLA was calculated as:

$$BLA = \frac{1}{N-2}\sum_{i=1}^{N-2}(-1)^{i+1}\left(d_{i+1,i+2} - d_{i,i+1}\right) \quad (16)$$

where $d_{i,j}$ is the interatomic distance between carbons *i* and *j*. A positive value of the BLA indicates a dominant aromatic character of the conjugated linker, while BLA <0 reveals a dominant quinoid (charge transfer) character. A value equal to zero in **1**–**4** indicates that the aromatic and quinoid resonance forms equivalently contribute to the ground-state electronic structure according to a 2-state resonance picture.

Increasing the number of phenyl rings in compounds **1**–**4** concomitantly destabilizes the HOMO and stabilizes the LUMO, inducing a lowering of the energy gap. From compound **1** to **2**, the enlargement of the conjugation length strongly increases the dipole moment. Further addition of phenyl units in compounds **3** and **4** slightly lowers the dipole moment, due to a decrease in the efficiency of the charge transfer between the *N,N*-dimethylamino and dicyano-pyrazine units. This lowering of the quinoid character from **2** to **4** is evidenced by the decrease of the difference in the net charges of the D and A units, as well as by the increase of the BLA values from −0.026 to +0.024 Å.

Replacing the central phenyl ring in compound **4** by an acetylenic linker (compound **5**) gives rise to a larger donor-to-acceptor charge transfer and strongly enhances the molecular dipole, while introducing a second phenylacetylene unit (from compound **5** to **6**) has a weak impact. Finally, comparing the results calculated for compounds **7** and **8** shows that the position of the acetylenic bridge impacts the ground-state intramolecular charge transfer (ICT), a larger dipole being obtained with the triple bond closer to the *N,N*-dimethylamino donor units.

3.2. Linear optical properties

Due to the Λ-symmetry of the molecules, the two lowest-energy transitions, $S_0 \rightarrow S_1$ and $S_0 \rightarrow S_2$, are optically allowed. The transition energies, wavelengths, oscillator strengths, as well as the main electronic excitations contributing to these two optical transitions, are gathered in Table 2. The experimental and calculated UV/Vis spectra are provided in Figs. S1 and S6. In all compounds, the $S_0 \rightarrow S_2$ transition is 0.1–0.2 eV higher in energy than $S_0 \rightarrow S_1$, and associated to a larger oscillator strength. As already observed for Λ-shape compounds such as 3,5-dinitroaniline [24] or 1,3-diamino-4,6-dinitrobenzene [19] derivatives, the transition dipole moment associated to the $S_0 \rightarrow S_1$ excitation ($\vec{\mu}_{01}$) is parallel to the transverse *x*-axis, while the one corresponding to $S_0 \rightarrow S_2$ ($\vec{\mu}_{02}$) is aligned along the C_2 symmetry axis (see Figs. S7 and S8). As discussed below, these two perpendicular charge-transfer excitations are responsible for the 2D NLO character of the chromophores.

Although the computed transition wavelengths globally underestimate the experimental absorption maximum, DFT calculations using the vertical approximation reproduce well the relative trends. Within the **1**–**4** series, the transition wavelength increases from **1** to **2**, and then decreases when introducing additional 1,4-phenylene units in

Table 1
Bond length alternation (BLA, Å), torsional angles (θ_{1-3}, deg.), HOMO and LUMO energies (eV), HOMO-LUMO gap (E_g, eV), ground-state dipole moment (μ_g, D), and sum of Mulliken charges within the dicyano-pyrazine and *N,N*-dimethylamino units (δ_A and δ_D, |e|), calculated at the IEF-PCM/M06–2X/6-311+G(d) level in dichloromethane.

Compound	BLA	$\theta_1, \theta_2, \theta_3$	HOMO	LUMO	E_g	μ_g	δ_A	δ_D
1	/	/	−7.39	−1.40	5.98	13.81	−1.46	1.46
2	−0.026	36	−6.58	−1.89	4.70	17.84	−0.92	1.05
3	0.014	39, 34	−6.57	−2.14	4.43	17.23	−1.00	0.92
4	0.024	40, 38, 35	−6.56	−2.20	4.36	16.68	−0.85	0.82
5	0.049	40	−6.50	−2.27	4.23	19.26	−0.95	1.03
6	0.060	41	−6.46	−2.37	4.10	19.50	−0.87	0.97
7	0.045	41, 35	−6.55	−2.34	4.21	17.93	−0.85	0.81
8	0.045	40, 36	−6.47	−2.24	4.23	19.22	−0.76	0.98

Table 2
Experimental maximum absorption wavelengths (λ_{exp}, nm), and wavelengths (λ_{ge}, nm), energies (ΔE_{ge}, eV), squared transition dipoles (μ^2_{ge}, a.u.^{2}) oscillator strengths (f_{ge}), photoinduced charge displacements (Δq, |e|), charge transfer distances (Δr,Å), dipole moment variations ($\Delta\mu_{ge}$, D), and weights of the main electronic excitations (≥10%), calculated at the IEF-PCM/M06–2X/6-311+G(d) level in dichloromethane for the two lowest-energy optical transitions.

Compound	λ_{exp} [29]	λ_{ge}	ΔE_{ge}	μ^2_{ge}	f_{ge}	Δq	Δr	$\Delta\mu_{ge}$	Electronic excitations
1:$S_0 \rightarrow S_1$	355	323	3.84	3.92	0.37	0.55	2.34	6.21	98% H→L
1:$S_0 \rightarrow S_2$		317	3.91	4.41	0.42	0.47	0.71	1.60	98% H→L+1
2:$S_0 \rightarrow S_1$	471	421	2.94	7.31	0.53	0.77	3.29	12.14	92% H→L
2:$S_0 \rightarrow S_2$		398	3.11	7.57	0.58	0.76	2.95	10.84	94% H→L+1
3:$S_0 \rightarrow S_1$	425	399	3.11	9.07	0.69	0.87	4.64	19.49	77% H→L + 10% H-2→L
3:$S_0 \rightarrow S_2$		376	3.30	15.37	1.24	0.86	4.72	19.35	53% H→L+1 + 29% H-1→L + 10% H-2→L+1
4:$S_0 \rightarrow S_1$	402	371	3.35	10.29	0.84	0.85	5.68	23.19	57% H→L + 26% H-2→L
4:$S_0 \rightarrow S_2$		355	3.49	16.75	1.43	0.89	6.10	26.09	43% H-1→L + 26% H→L+1 + 15% H-2→L+1
5:$S_0 \rightarrow S_1$	433	416	2.98	13.93	1.02	0.84	5.13	20.78	72% H→L + 10% H-2→L
5:$S_0 \rightarrow S_2$		392	3.17	23.90	1.85	0.84	5.35	21.60	45% H-1→L + 34% H→L+1
6:$S_0 \rightarrow S_1$	402	400	3.10	22.93	1.74	0.73	6.14	21.46	43% H→L + 21% H-2→L
6:$S_0 \rightarrow S_2$		387	3.20	39.56	3.10	0.74	6.50	22.92	36% H-1→L + 17% H→L+1 + 14% H→L+3 + 13% H-1→L+1
7:$S_0 \rightarrow S_1$	404	391	3.17	16.50	1.28	0.77	5.76	21.34	49% H→L + 27% H-2→L
7:$S_0 \rightarrow S_2$		373	3.28	28.06	2.28	0.80	6.36	24.24	39% H-1→L + 21% H→L+1 + 11% H-2→L+1
8:$S_0 \rightarrow S_1$	400	381	3.26	14.13	1.13	0.80	6.39	24.61	52% H→L + 19% H-2→L
8:$S_0 \rightarrow S_2$		368	3.37	29.74	2.45	0.82	6.74	26.46	43% H-1→L + 19% H→L+1 + 11% H-1→L+2 + 11% H→L+3

compounds **3** and **4**. The energy differences between the S_1 and S_2 excited states for compounds **1** to **3** are, in order, equal to 0.07, 0.17 and 0.19 eV. Interpreted using a Valence-Bond or Essential-State model, this increase can be ascribed to the strengthening of the interaction between the two branches of the molecules. In compound **4**, the splitting between the two first excited states reduces to 0.14 eV, suggesting a lowering in the strength of the interaction. Reversely, the transition probabilities toward the S_1 and S_2 states regularly increases from **1** to **4**, according to the increase of the transition dipole moments. This increase is particularly marked for transition dipoles associated to the $S_0 \rightarrow S_2$ excitation, which are aligned parallel to the charge transfer axis of the molecules.

Compared to compound **5**, the addition of a second phenylacetylene unit in compound **6** blue-shifts the first (second) absorption band by 0.12 (0.03) eV, and reduces the splitting between S_1 and S_2 from 0.19 to 0.10 eV. The strengths of the $S_0 \rightarrow S_1$ and $S_0 \rightarrow S_2$ transitions are also strongly increased. A slight blue-shift of the two absorption bands is also observed from **7** to **8**, showing that the position of the triple bond within the conjugated branches impact the vertical transition energies, but without any change in the S_1-S_2 gap. Note that the $S_0 \rightarrow S_1$ transition probability decreases while that of the $S_0 \rightarrow S_2$ transition slightly increases going from **7** to **8**.

As expected for push–pull conjugated dyes of C_2 symmetry, the $S_0 \rightarrow S_1$ absorption band is dominated by a $\pi \rightarrow \pi^*$ electronic transition between the highest occupied molecular orbital (HOMO, H) and lowest unoccupied molecular orbital (LUMO, L), while the $S_0 \rightarrow S_2$ is dominated by H-1→L and H→L+1 electronic excitations. As illustrated in Fig. 3, the HOMOs are delocalized over the donor moiety of the pyrazine derivatives, whereas the LUMOs are spread over the acceptor one, revealing a significant intramolecular charge transfer upon light excitation. However, the evolution observed in the transition energies do not always follow the evolution of the HOMO-LUMO gap, since other electronic excitations do contribute to the $S_0 \rightarrow S_1$ and $S_0 \rightarrow S_2$ absorption bands.

To gain better insight on the ICT occurring upon the excitation process, Fig. 3 also illustrates the difference between the total electron densities of the ground and excited state:

$$\Delta\rho = \rho_{S_1} - \rho_{S_0} = \Delta\rho^+ + \Delta\rho^- \quad (17)$$

where $\Delta\rho^+ > 0$ and $\Delta\rho^- < 0$ correspond to increasing and decreasing areas of the electron density, respectively. In line with previous studies on rod–like push–pull compounds [40–42], the photo–induced charge displacement (reported in Table 2) is evaluated as:

$$\Delta q = \int \Delta\rho^+(\mathbf{r})d\mathbf{r} = -\int \Delta\rho^-(\mathbf{r})d\mathbf{r} \quad (18)$$

While the charge transfer distance Δr is assimilated to the distance between the centroids of the $\Delta\rho^+$ and $\Delta\rho^-$ volumes. The change in dipole moment upon light excitation can then be expressed as $\Delta\mu_{ge} = \Delta q \times \Delta r$. As reported in Table 2, the $\Delta\mu_{ge}$ values increase with the length of the conjugated linker for both the S_1 and S_2 states. This enhancement is particularly marked in the **1**–**4** series of compounds, and mainly originates from the regular increase of the charge transfer distances Δr, while Δq values saturate from compound **3** to **4**. A similar enhancement of $\Delta\mu_{ge}$ values, although of weaker amplitude, is observed upon addition of a phenylacetylene unit from **5** to **6**. We also note that the photo-induced charge displacement is slightly larger in compound **8** than in compound **7** for both the S_1 and S_2 states.

3.3. Nonlinear optical properties

The results calculated at the IEF-PCM/M06–2X/6-311+G(d) level, for an incident wavelength λ of 1064 nm and in the static limit ($\lambda = \infty$), are collected in Table 3. The independent non-negligible components of the static first hyperpolarizability tensor are gathered in Table S1. Before analyzing the data, it is interesting to assess if the present family of compounds could be treated as having a planar C_{2v} symmetry, as assumed in earlier works for other Λ-shaped chromophores [24,25,28]. The contribution of the out-of-plane components to the total HRS hyperpolarizability can be evaluated by comparing the full β_{HRS} value to the one evaluated by using equation (8). As reported in Table 3, the $\beta_{HRS}(C_{2v})$ values differ from the full β_{HRS} values by about −20% for all compounds, except **1** and **8** for which the differences reach −27% and −14%, respectively. These results evidence that assuming a planar C_{2v} symmetry would not be fully justified for the compounds investigated here.

The data collected in Table S1 also show that the ratio between the main transverse and longitudinal components, $R = \beta_{zxx}/\beta_{zzz}$, decreases as increasing the length of the conjugated linker, both in the **1**–**4** molecular series and from **5** to **6**. The R value also decreases significantly from compound **7** to **8**, as the acetylenic bridge is shifted from position 2 to position 3 with respect to the pyrazine unit. It is also informative to rely on the Sum-Over-States (SOS) formalism to address the individual contributions of the low-lying excited states S_1 and S_2 to the two main

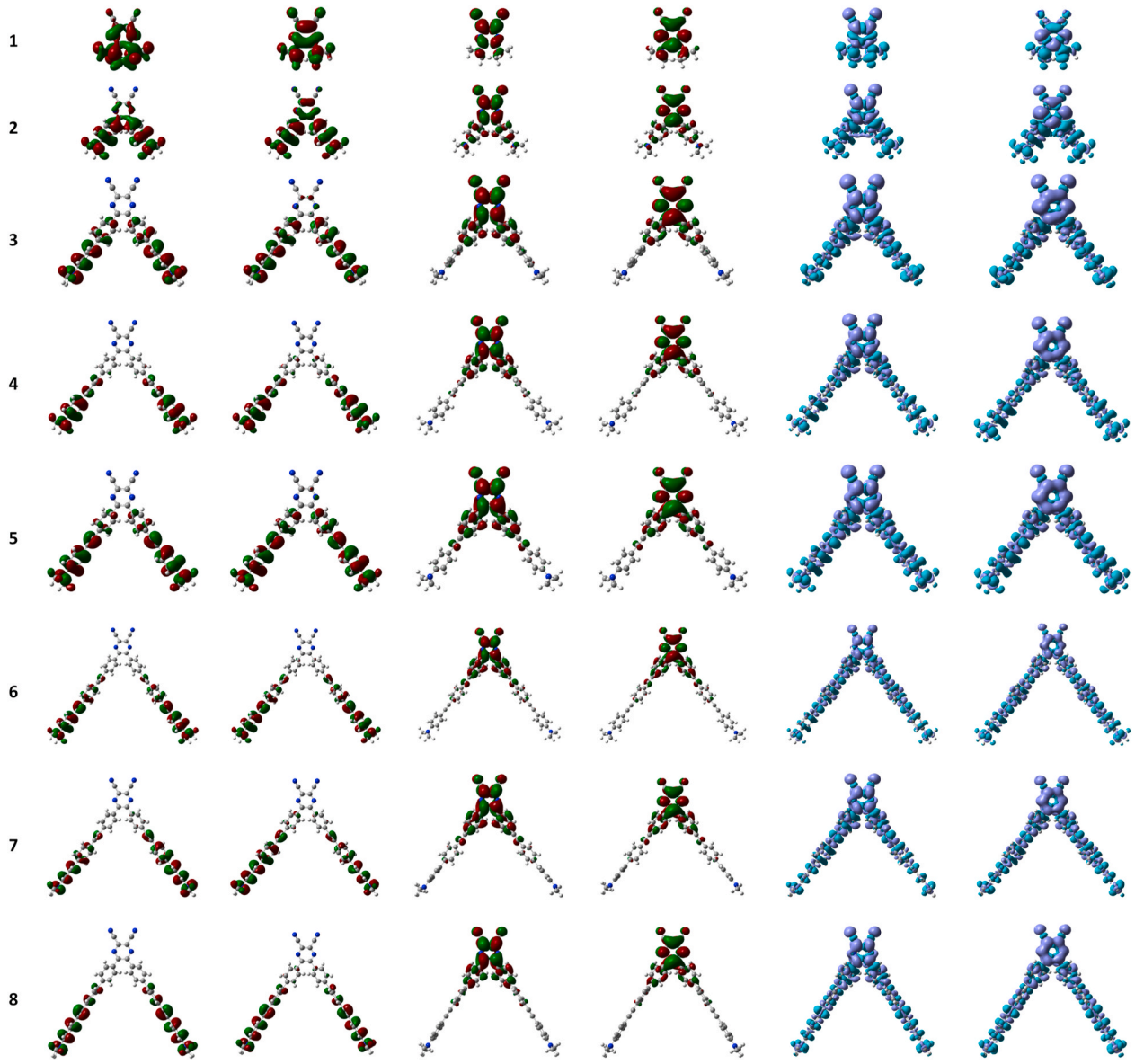

Fig. 3. From left to right: HOMO-1, HOMO, LUMO and LUMO+1 of the eight pyrazine derivatives, and electron density differences associated to the $S_0 \rightarrow S_1$ and $S_0 \rightarrow S_2$ transitions. Dark (light) blue lobes in density maps are associated with positive (negative) $\Delta\rho$ values.

Table 3
Static and dynamic HRS data calculated at the IEF-PCM/M06–2X/6-311+G(d) level in dichloromethane: first hyperpolarizability (β_{HRS}), anisotropy ratio (ρ) and depolarization ratio (*DR*). $\beta_{HRS}(C_{2v})$ values are calculated using equation (8), with deviations with respect to the full β_{HRS} values given in parentheses. All first hyperpolarizability values are reported in a.u. according the T convention [43]. 1 a.u. of $\beta = 3.6213 \times 10^{-42}\ m^4V^{-1} = 3.2064 \times 10^{-53}\ C^3m^3J^{-2} = 8.639 \times 10^{-33}$ esu.

	Calc. ($\lambda = \infty$)				Calc. ($\lambda = 1064$ nm)		
Compound	β_{HRS}	ρ	*DR*	$\beta_{HRS}(C_{2v})$	β_{HRS}	ρ	*DR*
1	1386	0.79	5.11	1010 (−27%)	1386	0.67	5.75
2	10685	0.68	5.69	8366 (−22%)	18291	0.52	6.64
3	15492	0.65	5.85	12489 (−19%)	30603	0.58	6.24
4	13286	0.65	5.85	10701 (−19%)	25744	0.61	6.07
5	25678	0.66	5.81	20403 (−21%)	59990	0.61	6.09
6	30752	0.63	5.97	24987 (−19%)	83428	0.57	6.33
7	21955	0.65	5.87	17682 (−19%)	53742	0.58	6.27
8	21181	0.58	6.28	18322 (−14%)	48496	0.50	6.74

first hyperpolarizability components. Since the $S_0 \rightarrow S_2$ excitation is associated to a transition dipole moment ($\overrightarrow{\mu}_{02}$) parallel to the C_2 axis, and since the dipole moment difference ($\Delta\overrightarrow{\mu}_{02}$) is oriented along the same axis due to the molecular symmetry, only the S_2 state contributes to the β_{zzz} component according to the following expression:

$$\beta_{zzz}^{S_2} = 6\frac{\mu_{02}^2 \Delta\mu_{02}}{\Delta E_{02}^2} \quad (19)$$

Similarly, the S_1 state contributes to the β_{zxx} component since $\overrightarrow{\mu}_{01}$ and $\Delta\overrightarrow{\mu}_{01}$ are respectively oriented perpendicular and parallel to the symmetry axis:

$$\beta_{zxx}^{S_1} = 2\frac{\mu_{01}^2 \Delta\mu_{01}}{\Delta E_{01}^2} \quad (20)$$

Note that the S_2 state also contributes to β_{zxx} through a cross-term (not considered here) implying the dipolar coupling with S_1:

$$\beta_{zxx}^{S_1/S_2} = 4\frac{\mu_{01}\mu_{12}\mu_{02}}{\Delta E_{01}\Delta E_{02}} \quad (21)$$

where $\mu_{12} = \langle 1 \left| \widehat{\mu}_x \right| 2 \rangle$ and $\widehat{\mu}_x$ is the dipole moment operator along x. Although the values of $\beta_{zxx}^{S_1}$ and $\beta_{zzz}^{S_2}$ (calculated using spectroscopic data of Table 2) correlate with the full β_{zxx} and β_{zzz} components (see Table S1 and Fig. S9), the two sets of values differ significantly, which evidence that the two main components of the β tensor cannot be reduced to the sole contributions of the low-lying S_1 and S_2 states.

We continue the discussion by comparing the theoretical results with experimental measurements. The HRS data of the eight investigated pyrazine derivatives, as measured in DCM solutions, are reported in Table 4. 3D representations of the scattered light as a function of the incident power and chromophore concentration (equation (1)), as well as polarization scans of $I_{\Psi V}^{2\omega}$ at constant incident power (equation (15)) are reported in Figs. S2–S5. Note that NLO measurements for some compounds are subject to significant errors due to two-photon induced fluorescence effects overlapping with the HRS signal. Fig. 4 compares the experimental and theoretical results, and illustrates the evolution of β_{HRS} and DR values within three subgroups of compounds presenting progressive structural variations, {**1**–**4**}, {**2**,**5**,**6**} and {**7**–**8**}.

Within the {**1**–**4**} series, elongating the conjugation path from **1** to **3** leads to a significant enhancement of β_{HRS}, while further addition of a phenylene linker in compound **4** is detrimental to the HRS response. Compared to experiments, both static and dynamic TDDFT calculations underestimate the HRS responses of the compounds, but reproduce well the trend. This non monotonic evolution of β_{HRS} results from a combination of different effects, which can be interpreted with the help of the SOS expressions (equations (19) and (20)) and the computational results collected in Table 2. From **1** to **2**, the increase of β_{HRS} originates from the decrease of the excitation energies towards the S_1 and S_2 states, combined with the increase of the dipole moment differences ($\Delta\mu_{ge}$) and transition dipole moments (μ_{ge}). From **2** to **3**, β_{HRS} increases despite the blueshift of the low-lying absorption bands, because of the large enhancement of μ_{ge} and $\Delta\mu_{ge}$ values. Finally, the lowering of β_{HRS} from **3** to **4**, well predicted by TDDFT calculations, cannot be rationalized by assuming that only the S_1 and S_2 states contribute to the first hyperpolarizability. Indeed, equations (19) and (20) predict an increase of the longitudinal and transverse β components, revealing significant (negative) contributions of higher energy excited states or possibly of the $\beta_{zxx}^{S_1/S_2}$ coupling term (equation (21)).

It is also worth noticing that the evolution of β_{HRS} from **1** to **4** also follows that of the molar extinction coefficient (ε_λ) measured at the harmonic wavelength ($\lambda = 532$ nm), which increases from 0 to 3000 and 3500 L mol^{-1} cm^{-1} from **1** to **3**, and then decreases to 750 L mol^{-1} cm^{-1} for **4**. Although absorption losses at the second harmonic wavelength are accounted for through a corrective term in equation (1), the slight overlap of the absorption band edge and the scattered light suggests that frequency dispersion effects also contribute to (and reinforce) the non monotonic evolution of β_{HRS} with the number of 1,4-phenylene rings in the linker. This is confirmed when comparing the evolution with the molecular size of the computed static and dynamic HRS hyperpolarizabilities (Fig. 4, top left panel).

Experimental anisotropy and depolarization ratios of chromophores **1**–**4**, respectively smaller than 1 and close to 5, indicate that the dipolar component of β is larger than the octupolar one. TDDFT calculations also predict a dominant dipolar character of the second-order NLO responses, although the calculated DR values are systematically larger than the measured ones. This dipolar character is further illustrated in Fig. 5, which provides a unit-sphere representation (USR) of the calculated static first hyperpolarizability [44,45] (see SI for details). As previously evidenced for a C_2-symmetric push-pull bifluorene derivative [46], the effective dipoles are oriented along the charge-transfer axes of the two molecular branches, which gives a helmet-like shape to the projection of the β tensor onto the pyrazine plane.

Importantly, the DR_{NK} values estimated for compounds **3** and **4** are much larger than the ones obtained assuming Kleinman symmetry, and reach values larger than 5, in closer agreement with the calculations. This result evidences the limit of applicability of the Kleinman approximation when the frequency of the incident optical field approaches the two-photon resonance. Such deviations from index permutation symmetry have been previously reavealed by means of polarization dependent electric field-induced second harmonic generation and electrooptical absorption measurements for other Λ-shaped derivatives, and were attributed to the presence of the low-lying perpendicular transitions [24]. They are further illustrated here by the calculated dynamic values of the β_{zxx} and β_{xxz} components (Table S2), which significantly differ from each other.

We now consider the {**2**,**5**,**6**} series. Comparing compounds **2** and **5**,

Table 4
HRS data measured in dichloromethane: first hyperpolarizability (β_{HRS}), anisotropy ratio (ρ), depolarization ratios estimated with (DR) and without (DR_{NK}) assuming Kleinman symmetry, and deviation from Kleinman (δ_{NK}, see equation (15)). $\Delta_{DR} = (DR_{NK} - DR)/DR$. First hyperpolarizability values are reported in a.u. according the T convention [43]. 1 a.u. of $\beta = 3.6213 \times 10^{-42}$ m^{4}V$^{-1} = 3.2064 \times 10^{-53}$ C^{3}m^{3}J$^{-2} = 8.639 \times 10^{-33}$ esu. Experimental errors are deduced from the fits (see SI).

Compound	β_{HRS}	ρ	DR	DR_{NK}	δ_{NK}	Δ_{DR}
1	4060 ± 210	0.85[a]	4.81	–	–	–
2	26700 ± 1350	0.86 ± 0.11[b]	4.81	–	–	–
3	41000 ± 2050	0.90 ± 0.02	4.64	5.46 ± 0.26	1.83 ± 0.53	0.18
4	32140 ± 1600	0.84 ± 0.02	4.89	5.44 ± 0.26	1.19 ± 0.50	0.11
5	40400 ± 2050	0.92 ± 0.02	4.56	5.66 ± 0.22	2.57 ± 0.47	0.24
6	37530 ± 1900	0.85 ± 0.02	4.85	5.50 ± 0.25	1.45 ± 0.49	0.13
7	36980 ± 1850	0.83 ± 0.02	4.94	5.79 ± 0.22	1.81 ± 0.42	0.17
8	17710 ± 890	1.04 ± 0.10[b]	4.13	4.10 ± 0.70	0.09 ± 1.63	−0.01

[a] Conjectured owing to the very weak HRS signal.
[b] Large errors are due to two-photon fluorescence.

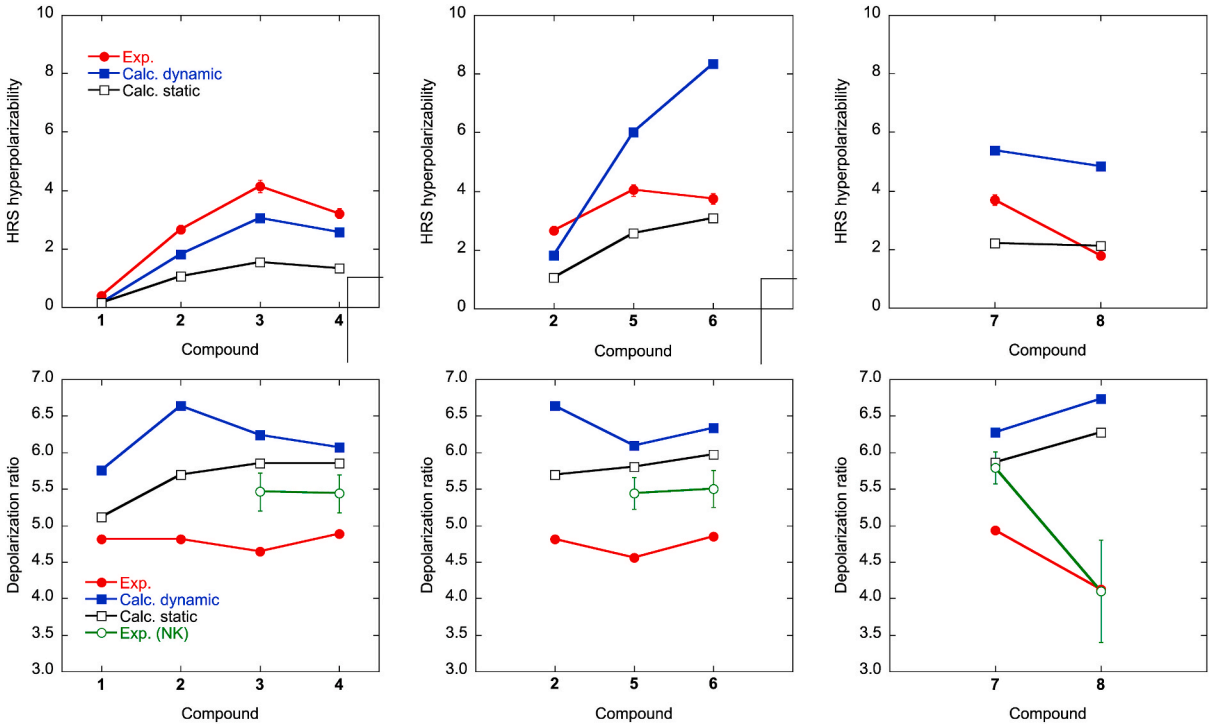

Fig. 4. Evolution of the HRS hyperpolarizability (in 10^4 a.u., top) and depolarization ratio (bottom) in the series of compounds **1**–**4** (left), **2**,**5**,**6** (middle) and **7**–**8** (right).

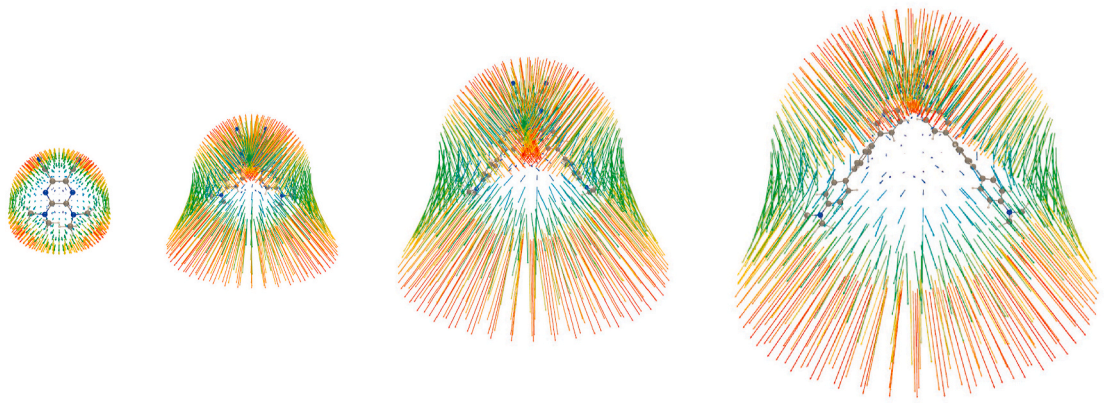

Fig. 5. Unit-sphere representation of the static first hyperpolarizability calculated at the TDDFT/M06–2X/6-311+G(d) for compounds **1** to **4** (from left to right). Arrows represent the magnitude of the second-order contribution to the induced dipole when an external field is applied normally to the surface of a virtual sphere centered on the center of mass of the molecules. See SI and Fig. S10 for details on the USR and color scales.

the addition of a phenylacetylene unit enhances β_{HRS} by a factor of 2.7, which is also reproduced by the calculations that predict an enhancement ratio of 3.3 and 2.4 of dynamic and static responses, respectively. This strong enhancement originates from the large increase of the transition dipole moments and of the dipole moment variations associated to these two electronic transitions (see Table 2). Adding a second phenylacetylene unit (from compound **5** to **6**) gives rise to a lowering (~7%) of β_{HRS}, which can be ascribed to the blueshift of the main absorption band. Although TDDFT calculations reproduce well the energy upshift of the $S_0 \rightarrow S_1$ and $S_0 \rightarrow S_2$ transitions, the lowering of β_{HRS} is not reproduced, because of the large increase of the strength of the transition towards the two excited states. Similarly to the **1**–**4** series, the magnitude of β_{HRS} correlates with the evolution of the molar extinction coefficient at the harmonic wavelength (ε_{532}~ 0, 4000 and 500 L mol^{-1} cm^{-1} for compounds **2**, **5** and **6**, respectively). The computed dynamic DR values are overestimated compared to experiments, but in global agreement with the experimental trend, showing a minimum for compound **5**. Here also, the non-Kleinman DR values estimated for compounds **5** and **6** are much closer from the computed ones.

Finally, we compare the NLO responses of compounds **7** and **8**, which incorporate three phenyl rings and one acetylenic bridge between the pyrazine unit and the terminal *N,N*-dimethylamino donor groups. The measured HRS hyperpolarizability is larger by 55% when the acetylenic linker is located in position 2 with respect to the pyrazine, which is consistent with a decrease of ε_{532} values (from ~500 to ~0 L mol^{-1} cm^{-1}). Although of much smaller amplitude (~10%), the lowering of β_{HRS} from **7** to **8** is reproduced by dynamic TDDFT calculations, and can be ascribed to the increase of the transition energies as well as to the decrease of the dipole of the $S_0 \rightarrow S_1$ transition. On the other hand, TDDFT calculations fail to reproduce the decrease of the DR from compound **7** to **8**. The unexpectedly low DR and DR_{NK} values measured for **8** might find origin in experimental errors due to large two-photon

fluorescence effects.

4. Conclusions

The second-order NLO responses of push-pull Λ-shaped pyrazine derivatives have been studied by means of HRS experiments and DFT calculations. This combination of techniques allowed to gain deep insight into the evolution of the first hyperpolarizabilities when varying the nature and length of the π-conjugated bridge linking the dicyanopyrazine acceptor unit to the *N,N*-dimethylamino donor groups. It is evidenced that the NLO responses of this series of compounds have a dominant dipolar character, and result from the additive contribution of two low-lying perpendicular electronic absorption bands. The largest structures exhibit large NLO responses, which points out the potential interest of these systems for optoelectronic applications. Results also clearly demonstrate that the second-order polarizability is not Kleinman-symmetric, and could not be finely interpreted assuming a planar C_{2v} symmetry for the molecular structures. More generally, this work illustrates the complementarity of experimental measurements and quantum chemical calculations for rationalizing the effects of structural symmetry, chemical modifications and two-photon resonance on the NLO properties of π-conjugated dyes.

CRediT authorship contribution statement

Frédéric Castet: Investigation, Conceptualization, Methodology, Formal analysis, Writing - original draft, Writing - review & editing. **Adrien Gillet:** Investigation. **Filip Bureš:** Resources, Writing - review & editing. **Aurélie Plaquet:** Investigation. **Vincent Rodriguez:** Conceptualization, Methodology, Formal analysis, Writing - original draft, Writing - review & editing. **Benoît Champagne:** Conceptualization, Methodology, Formal analysis, Writing - original draft, Writing - review & editing.

Declaration of competing interest

The authors declare that they have no known competing financial interests or personal relationships that could have appeared to influence the work reported in this paper.

Acknowledgment

V.R. is grateful to F. Adamietz for experimental support and technical developments, as well as to the CNRS and the Région Nouvelle Aquitaine for funding support. F.B. is indebted to the Ministry of Education, Youth and Sports of the Czech Republic (LTAIN19101). This work was also supported by funds from the Belgian Government (IUAP No. P7/5 "Functional Supramolecular Systems") and the Francqui Foundation. The calculations were performed on the computers of the *Consortium des Equipements de Calcul Intensif*, including those of the Technological Platform of High-Performance Computing, for which financial support from the FNRS-FRFC (Convention Nos. 2.4.617.07.F and 2.5020.11) is acknowledged, as well as on the *Mésocentre de Calcul Intensif Aquitain* (MCIA) of the University of Bordeaux, financed by the Conseil Régional d'Aquitaine and the French Ministry of Research and Technology.

Appendix A. Supplementary data

Supplementary data to this article can be found online at https://doi.org/10.1016/j.dyepig.2020.108850.

References

[1] Dalton LR, Sullivan PA, Bale DH. Electric field poled organic electro-optic materials: state of the art and future prospects. Chem Rev 2010;110(1):25–55.
[2] Stegeman GI, Stegeman RA. Nonlinear optics: phenomena, materials and devices. Hoboken, NJ: John Wiley and Sons; 2012.
[3] Campagnola PJ, Wei MD, Loew LM. High-resolution nonlinear optical imaging of live cells by second harmonic generation. Biophys J 1999;77:3341–9.
[4] Moreaux L, Sandre O, Charpak S, Blanchard-Desce M, Mertz J. Coherent scattering in multi-harmonic light microscopy. Biophys J 2001;80(3):1568–74.
[5] Dombeck DA, Blanchard-Desce M, Webb WW. Optical recording of action potentials with second-harmonic generation microscopy. J Neurosci 2004;24(4):999–1003.
[6] Reeve JE, Anderson HL, Clays K. Dyes for biological second harmonic generation imaging. Phys Chem Chem Phys 2010;12:13484–98.
[7] Marder SR, Beratan DN, Cheng L-T. Approaches for optimizing the first electronic hyperpolarizability of conjugated organic molecules. Science 1991;252(5002):103–6.
[8] Würthner F, Effenberger F, Wortmann R, Krämer P. Second-order polarizability of donor—acceptor substituted oligothiophenes: substituent variation and conjugation length dependence. Chem Phys 1993;173(2):305–14.
[9] Kanis DR, Ratner MA, Marks TJ. Design and construction of molecular assemblies with large second-order optical nonlinearities. quantum chemical aspects. Chem Rev 1994;94(1):195–242.
[10] Marder SR, Cheng L-T, Tiemann BG, Friedli AC, Blanchard-Desce M, Perry JW, Skindhøj J. Large first hyperpolarizabilities in push-pull polyenes by tuning of the bond length alternation and aromaticity. Science 1994;263(5146):511–4.
[11] Beckmann S, Etzbach K-H, Krämer P, Lukaszuk K, Matschiner R, Schmidt AJ, Schuhmacher P, Sens R, Seybold G, Wortmann R, Würthner F. Electrooptical chromophores for nonlinear optical and photorefractive applications. Adv Mater 1999;11(7):536–41.
[12] Plaquet A, Champagne B, Kulhánek J, Bureš F, Bogdan E, Castet F, Ducasse L, Rodriguez V. Effects of the nature and length of the π-conjugated bridge on the second-order nonlinear optical responses of push–pull molecules including 4,5-dicyanoimidazole and their protonated forms. ChemPhysChem 2011;12(17):3245–52.
[13] Castet F, Pic A, Champagne B. Linear and nonlinear optical properties of arylvinyldiazine dyes: a theoretical investigation. Dyes Pigments 2014;110:256–60.
[14] Klikar M, le Poul P, Ružička A, Pytela O, Barsella A, Dorkenoo KD, Robin-le Guen F, Bureš F, Achelle S. Dipolar nlo chromophores bearing diazine rings as π-conjugated linkers. J Org Chem 2017;82(18):9435–51.
[15] Parthasarathy V, Pandey R, Das PK, Castet F, Blanchard-Desce M. Linear and nonlinear optical properties of tricyanopropylidene-based merocyanine dyes: synergistic experimental and theoretical investigations. ChemPhysChem 2018;19(2):187–97.
[16] Kim HM, Cho BR. Second-order nonlinear optical properties of octupolar molecules structure–property relationship. J Mater Chem 2009;19:7402–9.
[17] Argouarch G, Veillard R, Roisnel T, Amar A, Boucekkine A, Singh A, Ledoux I, Paul F. Donor-substituted triaryl-1,3,5-triazinanes-2,4,6-triones: octupolar nlophores with a remarkable transparency–nonlinearity trade-off. New J Chem 2011;35:2409–11.
[18] Castet F, Blanchard-Desce M, Adamietz F, Poronik YM, Gryko DT, Rodriguez V. Experimental and theoretical investigation of the first-order hyperpolarizability of octupolar merocyanine dyes. ChemPhysChem 2014;15(12):2575–81.
[19] Nalwa HS, Nakajima K, Watanabe T, Nakamura K, Yamada A, Miyata S. Second-harmonic generation in Langmuir-blodgett monolayer of a two-dimensional charge-transfer molecule: N,n'-dioctadecyl-4,6-dinitro-1,3-diaminobenzene. Jpn J Appl Phys 1991;30(Part 1):983–9. No. 5.
[20] Hendrickx E, Boutton C, Clays K, Persoons A, van Es S, Biemans T, Meijer B. Quadratic nonlinear optical properties of correlated chromophores: cyclic 6,6'-dinitro-1,1'-binaphthyl-2,2'-ethers. Chem Phys Lett 1997;270(1):241–4.
[21] Deussen H-J, Boutton C, Thorup N, Geisler T, Hendrickx E, Bechgaard K, Persoons A, Bjørnholm T. New chiral bis(dipolar) 6,6'-disubstituted binaphthol derivatives for second-order nonlinear optics. Chem Eur J 1998;4(2):240–50.
[22] Sergeyev S, Didier D, Boitsov V, Teshome A, Asselberghs I, Clays K, Vande Velde C, Plaquet A, Champagne B. Symmetrical and nonsymmetrical chromophores with Tröger's base skeleton: chiroptical, linear, and quadratic nonlinear optical properties—a joint theoretical and experimental study. Chem Eur J 2010;16(27):8181–90.
[23] Kournoutas F, Fihey A, Malval J-P, Spangenberg A, Fecková M, le Poul P, Katan C, Robin-le Guen F, Bureš F, Achelle S, Fakis M. Branching effect on the linear and nonlinear optical properties of styrylpyrimidines. Phys Chem Chem Phys 2020;22:4165–76.
[24] Wortmann R, Kramer P, Glania C, Lebus S, Detzer N. Deviations from kleinman symmetry of the second-order polarizability tensor in molecules with low-lying perpendicular electronic bands. Chem Phys 1993;173(1):99–108.
[25] Moylan CR, Ermer S, Lovejoy SM, McComb I-H, Leung DS, Wortmann R, Krdmer P, Twieg RJ. (dicyanomethylene)pyran derivatives with c2v symmetry: an unusual class of nonlinear optical chromophores. J Am Chem Soc 1996;118(51):12950–5.
[26] Liu Y, Liu Y, Zhang D, Hu H, Liu C. Theoretical investigation on second-order nonlinear optical properties of (dicyanomethylene)-pyran derivatives. J Mol Struct 2001;570(1):43–51.
[27] Yang M, Champagne B. Large off-diagonal contribution to the second-order optical nonlinearities of λ-shaped molecules. J Phys Chem A 2003;107(19):3942–51.
[28] Ostroverkhov V, Petschek R, Singer K, Twieg R. λ-like chromophores for chiral nonlinear optical materials. Chem Phys Lett 2001;340(1):109–15.
[29] Bureš F, Čermáková H, Kulhánek J, Ludwig M, Kuznik W, Kityk IV, Mikysek T, Ružička A. Structure—property relationships and nonlinear optical effects in donor-substituted dicyanopyrazine-derived push–pull chromophores with enlarged and varied π-linkers. Eur J Org Chem 2012;3:529–38. 2012.

[30] Sanguinet L, Pozzo JL, Rodriguez V, Adamietz F, Castet F, Ducasse L, Champagne B. Acido- and photo-triggered NLO properties enhancement. J Phys Chem B 2005;109(22):11139–50.
[31] Castet F, Bogdan E, Plaquet A, Ducasse L, Champagne B, Rodriguez V. Reference molecules for nonlinear optics: a joint experimental and theoretical investigation. J Chem Phys 2012;136(2):024506.
[32] Bersohn R, Pao Y, Frisch HL. Double quantum light scattering by molecules. J Chem Phys 1966;45:3184–98.
[33] Johnson LE, Dalton LR, Robinson BH. Optimizing calculations of electronic excitations and relative hyperpolarizabilities of electrooptic chromophores. Acc Chem Res 2014;47(11):3258–65.
[34] Bondu F, Quertinmont J, Rodriguez V, Pozzo J-L, Plaquet A, Champagne B, Castet F. Second-order nonlinear optical properties of a dithienylethene–indolinooxazolidine hybrid: a joint experimental and theoretical investigation. Chem Eur J 2015;21(51):18749–57.
[35] Beaujean P, Bondu F, Plaquet A, Garcia-Amorós J, Cusido J, Raymo FM, Castet F, Rodriguez V, Champagne B. Oxazines: a new class of second-order nonlinear optical switches. J Am Chem Soc 2016;138(15):5052–62.
[36] Pielak K, Bondu F, Sanguinet L, Rodriguez V, Champagne B, Castet F. Second-order nonlinear optical properties of multiaddressable indolinooxazolidine derivatives: joint computational and hyper-Rayleigh scattering investigations. J Phys Chem C 2017;121(3):1851–60.
[37] Lescos L, Sitkiewicz S, Beaujean P, Blanchard-Desce M, Champagne BR, Matito E, Castet F. Performance of DFT functionals for calculating the second-order nonlinear optical properties of dipolar merocyanines. Phys Chem Chem Phys 2020: 16579–94.
[38] Tomasi J, Mennucci B, Cammi R. Quantum mechanical continuum solvation models. Chem Rev 2005;105(8):2999–3094.
[39] Frisch MJ, Trucks GW, Schlegel HB, Scuseria GE, Robb MA, Cheeseman JR, Scalmani G, Barone V, Mennucci B, Petersson GA, Nakatsuji H, Caricato M, Li X, Hratchian HP, Izmaylov AF, Bloino J, Zheng G, Sonnenberg JL, Hada M, Ehara M, Toyota K, Fukuda R, Hasegawa J, Ishida M, Nakajima T, Honda Y, Kitao O, Nakai H, Vreven T, Montgomery Jr JA, Peralta JE, Ogliaro F, Bearpark M, Heyd JJ, Brothers E, Kudin KN, Staroverov VN, Kobayashi R, Normand J, Raghavachari K, Rendell A, Burant JC, Iyengar SS, Tomasi J, Cossi M, Rega N, Millam JM, Klene M, Knox JE, Cross JB, Bakken V, Adamo C, Jaramillo J, Gomperts R, Stratmann RE, Yazyev O, Austin AJ, Cammi R, Pomelli C, Ochterski JW, Martin RL, Morokuma K, Zakrzewski VG, Voth GA, Salvador P, Dannenberg JJ, Dapprich S, Daniels AD, Farkas Ö, Foresman JB, Ortiz JV, Cioslowski J, Fox DJ. Gaussian 09 revision A.02. Wallingford CT: gaussian Inc.; 2009.
[40] Le Bahers T, Adamo C, Ciofini I. A qualitative index of spatial extent in charge-transfer excitations. J Chem Theor Comput 2011;7(8):2498–506.
[41] Ciofini I, Le Bahers T, Adamo C, Odobel F, Jacquemin D. Through-space charge transfer in rod-like molecules: lessons from theory. J Phys Chem C 2012;116(22): 11946–55.
[42] Orlowski R, Banasiewicz M, Clermont G, Castet F, Nazir R, Blanchard-Desce M, Gryko DT. Strong solvent dependence of linear and non-linear optical properties of donor-acceptor type pyrrolo[3,2-b]pyrroles. Phys Chem Chem Phys 2015;17: 23724–31.
[43] Willetts A, Rice JE, Burland DM, Shelton DP. Problems in the comparison of theoretical and experimental hyperpolarizabilities. J Chem Phys 1992;97(10): 7590–9.
[44] Tuer A, Krouglov S, Cisek R, Tokarz D, Barzda V. Three-dimensional visualization of the first hyperpolarizability tensor. J Comput Chem 2011;32(6):1128–34.
[45] Liégeois V. Drawmol, uNamur. www.unamur.be/drawmol.
[46] Castet F, Lerychard T, Pielak K, Szalóki G, Dalinot C, Leriche P, Sanguinet L, Champagne B, Rodriguez V. How dimerization through a spiro junction modifies the nonlinear optical properties of a push–pull organic dye: insights from theory and hyper-Rayleigh scattering. ChemPhotoChem 2017;1(3):93–101.